Progress In Electromagnetics Research C, Vol. 82, 145–153, 2018

Compact QMSIW Based Antennas for WLAN/WBAN Applications

Divya Chaturvedi* **and Singaravelu Raghavan**

Abstract—In this paper, two compact planar substrate integrated waveguide (SIW) cavity-backed antennas are proposed for wireless local area network (WLAN) at 5.5 GHz and wireless body area network (WBAN) at 5.8 GHz. The miniaturization is achieved with the concept of quarter-mode-topology, and the size of the cavity is reduced up to one-fourth of the circular SIW cavity. A L-shaped slot is etched on the top plane for miniaturization, and antenna-1 is realized which resonates at 5.5 GHz. A metal strip has been added in the middle section of the slot, and antenna-2 is realized, which resonates at 5.8 GHz. Both proposed antennas are tested in free space, while the performance of antenna-2 is investigated for on-body condition. In free space, the measured impedance bandwidths of the antenna are 160 MHz and 210 MHz at 5.5 GHz and 5.8 GHz, respectively. The radiation efficiency of the antenna is 89.4% in free space and 57% on phantom at 5.8 GHz. Both measured and simulated results are observed, and they are in a good agreement.

1. INTRODUCTION

Recently, the wireless body network has become a great area of research with the development of wearable gadget such as a smart watch, where body wearable antennas can be fixed in small space. These types of antennas can be embedded in electronic equipment to utilize for diagnosis, real-time health-monitoring and telemetry applications [1, 2]. The essential requirements of on-body antennas are compact size, low profile and low sensitivity to the surrounding medium. On-body antennas have been widely implemented with the conventional microstrip patch technology [3]. However, these antennas suffer from the problems of frequency detuning, deterioration in efficiency, gain and radiation pattern in the proximity to the human body due to poor isolation from the surrounding [4]. In [5] a wearable antenna is implemented with a high impedance surface to minimize the loading effect and SAR, but the layered type of structure limits its deployment in the integration of the planar structure. The antennas implemented with Substrate Integrated Waveguide (SIW) technology are capable to overcome problems of the conventional antennas.

The SIW technology has attracted a lot of attention from the researchers due to its ascribed features of low losses, moderate power handling capability, and good isolation from the adjoining medium [6–8]. In the past decade, several microwave passive components have been developed in SIW technology by deploying its advantage of high-quality-factor [9, 10]. SIW is a closed cavity structure, which provides a high front-to-back ratio (FTBR), low losses due to suppression of surface waves as well as high isolation between the radiating part and surrounding medium [12]. SIW cavity offers the advantage of miniaturization by utilizing half-mode and quart-mode topology by maintaining similar cavity features. The cavity size can be reduced up to 50%, by utilizing half-mode substrate integrated waveguide (HMSIW). In HMSIW cavity one open edge acts as a dielectric aperture for radiation, while other edges are shielded by shorting vias. A few HMSIW based dual-band antennas are reported in [13–15], which have good radiation characteristics. Further, the size can be reduced by 75% with the deployment

Received 20 January 2018, Accepted 18 March 2018, Scheduled 28 March 2018
* Corresponding author: Divya Chaturvedi (divyanitt31@gmail.com).
The authors are with the Department of ECE, NIT Trichy, Tamilnadu-620 015, India.

of quarter-mode substrate integrated waveguide (QMSIW) [16, 17], where two open edges are used as dielectric aperture ,and remaining one edge is shorted with vias. In addition, the size reduction in the cavity has been achieved with eight modes, where frequency has been tuned at different frequencies depending on the rotation of the CSRR slot [18]. However, the overall size of the reported antenna has not been reduced compared to the proposed antenna due to the deployment of microstrip feeding technique.

Recently, a few SIW based antennas have been implemented on textile material to acquire the conforming ability on different types of platforms [19–21]. However, the performance of the proposed antenna is robust compared to the aforementioned antennas because fully textile fabrication often suffers fabric compression, flexing, and moistening.

In this paper, two prototypes based on QMSIW antennas are designed, where antenna-1 is proposed for WLAN (5.44–5.60 GHz), 160 MHz and antenna-2 for WBAN (5.68–5.89 GHz, ISM band), 210 MHz applications. A quarter-mode topology has been implemented, to reduce the size of the antenna by 75% of the conventional circular cavity [15]. The proposed antenna has the advantages of more compact size than [15, 16], due to the deployment of quarter-mode and coaxial feeding technique. It retains the cavity features of higher gain, better isolation than conventional patch antennas, and easy integration due to the planar structure.

2. ANTENNA DESIGN METHODOLOGY

The radius of circular SIW cavity is considered 'r', and its mode of operation is TM_{010}. The equation to design circular SIW cavity is shown in Equation (1) [17]

$$f_r = \frac{K_{mn}c}{2\pi r\sqrt{\mu_r\varepsilon_r}} \tag{1}$$

where c = velocity of light in free space; Bessel's function coefficient for the mode TM_{010} is $K_{mn} = 2.404$; μ_r and ε_r represent the relative permeability and permittivity of the substrate. For $r = 13.8$ mm, the resonant frequency of the FMSIW circular cavity for mode TM_{010} is calculated of 6.5 GHz, shown in Fig. 2.

The evolution of design process from full-mode (FM) to quarter-mode (QM) is exhibited in Fig. 1, and it is explained with the help of reflection coefficient plots in Fig. 2. The mode symmetry is present along the perfect magnetic conductor (PMC) walls A-A' and B-B', shown in Figs. 1(a), 1(b). The half-mode field distribution is achieved, when circular SIW cavity is bisected along the wall A-A' [16], and the resonant frequency shifts downward at 6.24 GHz [3] . It can be observed from Fig. 2 that bandwidth is enhanced in half-mode compared to full-mode cavity, due to an increasement in dielectric aperture area for radiations from open edge. Therefore, fringing field increases, and quality factor decreases, which leads to miniaturization and enhancement in the bandwidth [18]. Similarly, in the next step, when HMSIW cavity is bisected along the other PMC wall B-B', QM field distribution of TM_{010} mode is achieved, and the resonant frequency shifts at 5.8 GHz. The magnitudes of absolute E-field distributions of the dominant-mode resonant frequency in full-mode, half-mode and quarter-mode of circular SIW cavity are depicted in Fig. 3.

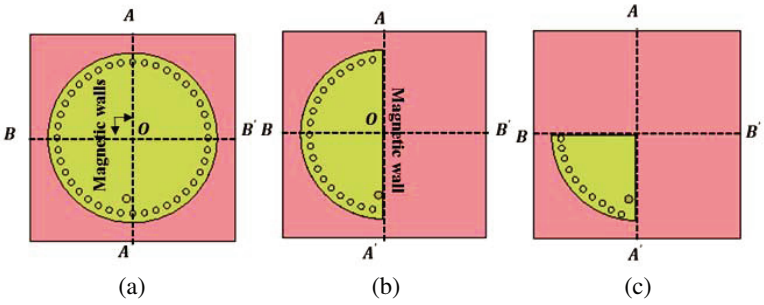

Figure 1. Antenna design evolution. (a) FMSIW circular cavity. (b) HMSIW. (c) QMSIW.

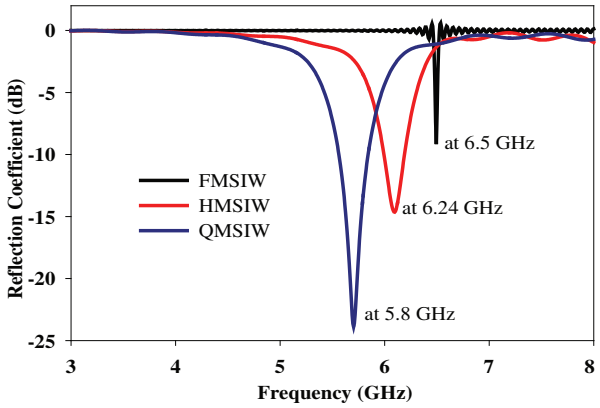

Figure 2. Reflection coefficients against frequency for FMSIW, HMSIW, and QMSIW.

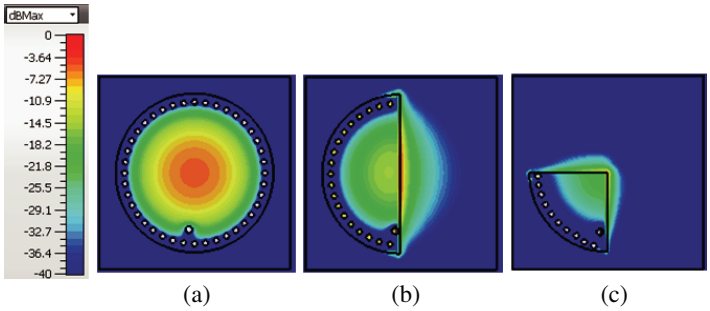

Figure 3. E-field distribution of the mode TM_{010}. (a) FMSIW. (b) HMSIW. (c) QMSIW.

In the next step for further miniaturization, an L-shaped slot of dimensions $0.2\lambda_g \times 0.14\lambda_g$ is etched on the top plane of the cavity. After introducing the slot, resonant frequency of the cavity shifts downward at 5.5 GHz, and it is named as antenna-1. The slot consists of identical sides 'l_{slot}' parallel to the radiating edges. The slot is etched with the aim to offer miniaturization, and it offers radiation in the same phase of the dielectric apertures, hence the field distribution of TM_{010} mode is not disturbed with the placement of slot. The slot adds series capacitance, which leads to shifting the operating frequency downward. In the next step, a metal strip is introduced in the middle section of slot which shifts the resonant frequency at 5.8 GHz, and it is named as antenna-2, shown in Fig. 4. The metal strip provides a direct shorting path to the current from magnetic walls to electric walls, hence the effect of slot becomes insignificant.

The proposed antennas consist of top cladding and bottom cladding connected through shorting vias. The overall size of the proposed antenna is $0.52\lambda_g \times 0.52\lambda_g$ for antenna-1 and $0.54\lambda_g \times 0.54\lambda_g$ for antenna-2. λ_g is the guiding wavelength at 5.5 GHz and 5.8 GHz, respectively) while conducting patch is 150 mm^2, fabricated on RT Duroid 5880 of thickness 1.57 mm ($\varepsilon_r = 2.2$ and loss tangent = 0.002). The cavity structure is shorted by vias from one side, and radiations take place from other open edges of the quarter-mode cavity. To avoid the leakage of energy from the side walls, SIW guidelines are taken into consideration, where $d_{via} = 1$, $S_{via} = 1.8$ are specified as per the conditions of Equation (2) [11]

$$d_{via}/s_{via} \geq 0.5 \text{ and } d_{via}/\lambda_o \leq 0.1 \tag{2}$$

The simulation studies of the proposed antennas are carried out using CST Microwave Studio Simulation Solver. A coaxial feeding technique is deployed mainly to achieve miniaturization. The coaxial feeding technique consists of less spurious radiation than microstrip feeding technique, which leads to high gain and good radiation characteristics. In order to design a coaxial feeding, a hole is drilled to short the inner copper pin of the diameter '$d_{in} = 0.655$ mm' to the patch. A circular slot of diameter '$d_{out} = 2.05$ mm' is etched on the ground plane to couple the electromagnetic energy to the cavity and to make characteristic impedance of 50 Ω.

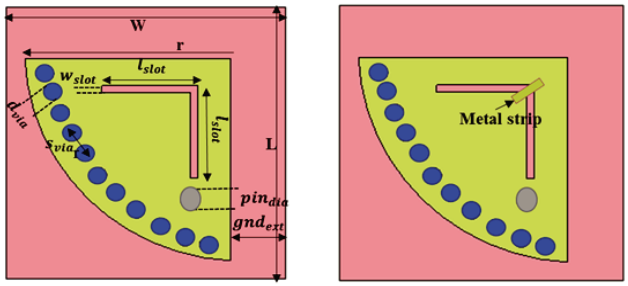

(a) (b)

Figure 4. (a) Configurations of antenna-1, and (b) antenna-2. Dimensions of the antenna specified in mm, $L = W = 19$, $r = 13.8$, $l_{slot} = 7$, $pin_{dia} = 1.25$, $gnd_{ext} = 3.5$, $d_{via} = 1$, $S_{via} = 1.8$, $w_{slot} = 0.5$.

3. RESULTS AND DISCUSSION IN FREE SPACE

Two antenna prototypes are realized from the QMSIW cavity, where antenna-1 is depicted without the metal strip and antenna-2 depicted with the metal strip, shown in Figs. 4(a) and 4(b). The resonant frequency of antenna-1 is obtained at 5.5 GHz due to miniaturization introduced by the slot. When the strip is absent, the impact of slot dominates, since the current path extends along the slot from open edges to shorted edge, and it resonates at 5.5 GHz, which is utilized here for WLAN application under the standard IEEE 802.11n. In antenna-2 when the metal strip is added in the middle position of the slot, it creates a short circuit path, and current travels directly from open edges towards vias, which is

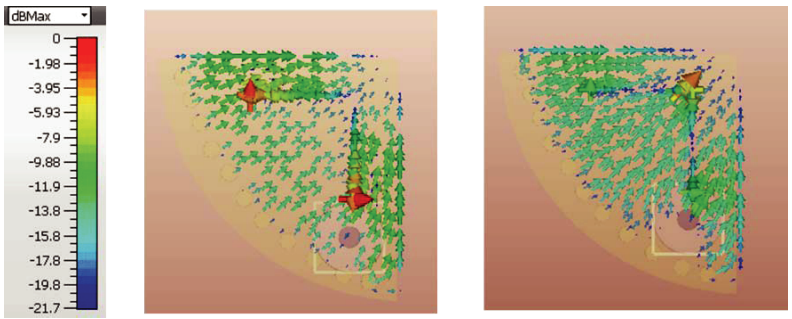

(a) (b)

Figure 5. Vector surface current distribution, (a) without metal strip, (b) with metal strip.

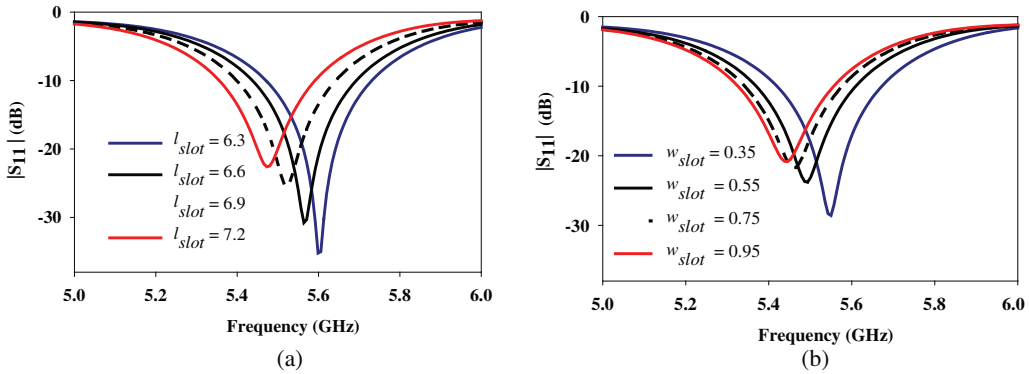

(a) (b)

Figure 6. Reflection coefficient plots with frequency for antenna-1, (a) with different lengths, (b) different slot widths.

conjectured as that there is no impact of the slot on the resonant frequency, shown in Fig. 4(b). This can be observed with the help of vector surface current distribution in Fig. 5. The performance of the antenna-2 is similar to the conventional QMSIW cavity with an increase in a gain value by 1.5 dBi. The enhancement in the peak gain value of antenna-2 compared to QMSIW cavity due to additional radiation from the slot.

A parametric study on the frequency by varying the length and width of the slot is illustrated in Fig. 6. If the length of slot increases, the operating frequency shifts downward because the loading of series capacitance increases. However, impedance matching deteriorates, and bandwidth remains constant. The L-shaped slot is a non-resonant slot, which maintains radiation characteristics of the quarter-mode cavity. Similarly, if the width of the slot increases frequency shifts downward, and impedance matching also deteriorates, but variation in operating frequency is much more significant with slot width than slot length. Both fabricated prototypes of the antenna are shown in Fig. 7. The antenna is fabricated through a copper etching process, and vias are shorted from top to bottom plane with the help of copper wires. A comparison detail of parameters for both the frequency bands is shown in Table 1.

Table 1. Antenna parameters vs frequency in free space.

Parameters	**Antenna-1 (5.5 GHz)**		**Antenna-2 (5.8 GHz)**	
	Sim.	**Meas.**	**Sim.**	**Meas.**
f_o (GHz)	5.49	5.52	5.83	5.8
BW (MHz)	210	160	240	210
Effic. (%)	89	NV	89.4	NV
Gain (dBi)	4.9	4.5	5.09	4.88

* NV — not verified

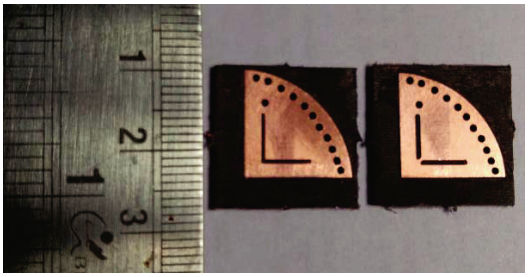

Figure 7. Fabricated prototypes of the antenna-1 and antenna-2.

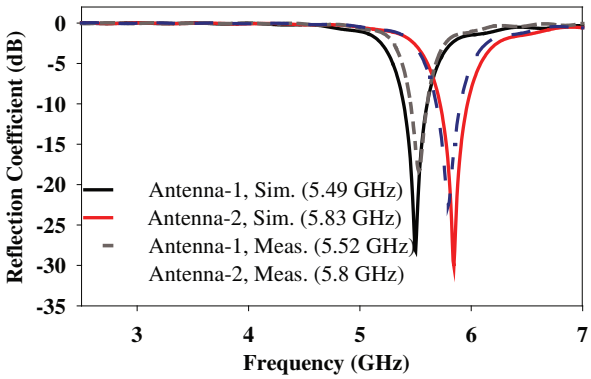

Figure 8. Reflection coefficient plots of the antenna-1 and antenna-2 in free space condition.

The measurements of the proposed antennas are carried out using Agilent E5071B (ENA Series) Network Analyzer, and the tested results are exhibited in Fig. 8. The simulated and measured impedance bandwidths of antenna-1 are (5.38–5.57 GHz) and (5.44–5.60 GHz) at the resonant frequencies of 5.49 and 5.52 GHz, respectively. While simulated and measured impedance bandwidths for antenna-2 are (5.71–5.97 GHz) and (5.68–5.89 GHz) at the resonances of 5.83 GHz and 5.8 GHz, respectively. A slight discrepancy in the measured reflection coefficients from simulations is attributed to the limitations of the fabrication process. The measured peak gains of the antenna at 5.5 GHz and 5.8 GHz are 4.5 and 4.88 dBi, respectively.

4. ANTENNA PERFORMANCE FOR ON-BODY CONDITIONS

Antenna-2 has been investigated for on-body conditions at 5.8 GHz. To investigate on-body antenna performance, antenna-2 is simulated on a multi-layered human body equivalent phantom, and the properties of various tissues, fat, skin, muscle and bone, are specified in Table 2. The measured reflection coefficient on the human arm slightly deviates from the simulation one, due to change in the dielectric properties of human arm tissues and body equivalent phantom. The impedance bandwidth and imposed return loss condition of $|S_{11}| < -10$ dB is maintained the same in measured results. The simulated impedance bandwidth of the proposed antenna-2 on a phantom is 217 MHz (5.750–5.967 GHz). The measured impedance bandwidth, when antenna-2 is tested on the human arm, is 228 MHz (5.663–5.891 GHz), which shows a slight enhancement in bandwidth by 11 MHz from the simulated result. The proposed antenna covers the complete Industrial Scientific & Medical band (5.725–5.875 GHz) with 78 MHz extra margin. The proposed antenna shows enhancement in the bandwidth of 30 MHz in the proximity to the human arm compared to the free space due to the loading effect introduced by the lossy human tissues, shown in Fig. 9.

Far-field radiation pattern plots are depicted in Fig. 10 at 5.5 GHz/5.8 GHz in free space and at 5.8 GHz on the phantom. The antenna radiation patterns at E-plane and H-plane are same because both open edges consist of the same length and perpendicular to each other. In the case of antenna-1, the maximum radiation is oriented towards $\phi = 3°$ with the peak gain of 4.5 dBi in both of the

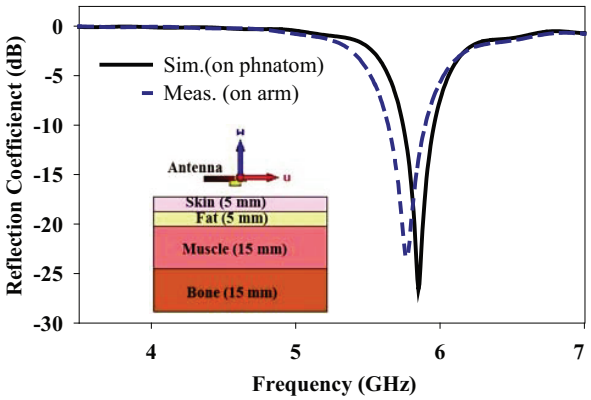

Figure 9. Simulated results on human body equivalent phantom and measured results on human arm.

Table 2. Dielectric properties of human body tissues at 5.8 GHz.

Body Tissues	Thickness (mm)	Permittivity (ε_r)	Conductivity (σ)
Bone	15	9.7	1.16
Muscle	10	48.4	4.92
Fat	5	4.85	0.33
Dry Skin	3.5	35.2	3.72

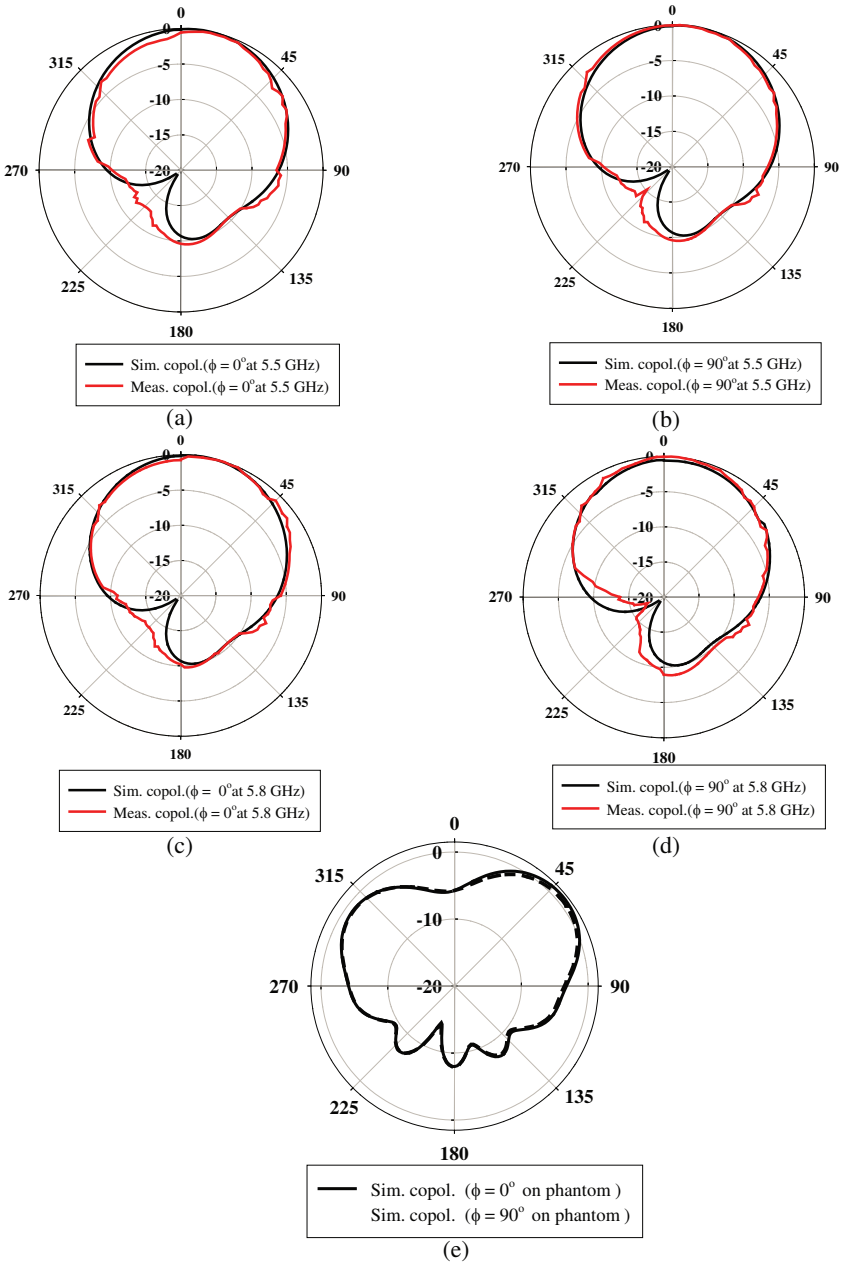

Figure 10. Normalized simulated and measured radiation pattern of antenna-1, antenna-2 (a), (b), (c), (d) H-plane ($\phi = 0°$) and E plane ($\phi = 90°$) in free space at 5.5 GHz, 5.8 GHz. (e) Simulated radiation pattern at E-plane and H-plane on body equivalent phantom at 5.8 GHz.

planes. Similarly, in the case of antenna-2, the maximum radiation is oriented towards $\phi = 3°$ with the peak gain of 4.88 dBi in both of the planes. The radiation pattern plots are similar at 5.5 GHz and 5.8 GHz because both resonant frequencies are possessed by the same mode TM_{010}. In free space, the beamwidth is narrower than on-phantom at 5.85 GHz, which represents the degradation of the peak gain from 5.09 dBi to 3.55 dBi on-phantom. The phantom consists of layers of high permittivity tissues, which are responsible for generating back lobes. The simulated antenna efficiency decreases dramatically from 89.4% in free space to 57% on the phantom because the output power is observed by phantoms, and the radiations are converted into heat [1]. The performance of the proposed antenna is compared with previously existing antennas in Table 3, and it can be observed that the proposed antennas have more compact size and comparable bandwidth compared to other prototypes.

Table 3. Performance comparison of the proposed antennas with Reference antennas.

Ref.	f_r (GHz)	Size (mm)	BW (%)	Gain (dBi)	Substrate	ε_r/Thickness (mm)	Year of publication
[2]	1.43	2886	7	0.8	RT5880	2.2/ 0.8	2014
[5]	2.44	1445	2.5	6.1	FR4	4.4/3	2015
[6]	5.8	1614	3.5	2	Arlon	2.7/1.524	2014
[17]	5.8	1927	5.9	6.25	RT5880	2.2/1.58	2017
[18]	5.08	1660	1.5	5.9	RT5880	2.2/1.58	2013
[19]	5.8	3150	4	3.12	Felt	1.2/1	2016
Antenna-1	5.5	361	2.9	4.5	RT5880	2.2/1.57	NA (not available)
Antenna-2	5.8	361	3.6	4.88	RT5880	2.2/1.57	NA

5. CONCLUSION

In this paper, two QMSIW antennas are proposed for WLAN and WBAN applications without and with the addition of metal strip in the middle position of an L-shaped slot. Both prototypes are tested in free space, and they show a close agreement. The performance of antenna-2 is tested on a human arm and found to be stable with respect to the phantom. The impedance bandwidth of the antenna is slightly increased in the proximity of the human arm compared to the free space, due to increase in losses. The proposed antenna maintains moderate efficiency and gain on the human arm in a very compact structure. The weakness of the proposed antenna is that it cannot be bent or crumpled since it is fabricated on a robust material. Hence it is suitable to use in medical equipment which directly comes in contact with the human body. The proposed antenna has the advantages of very compact size, low profile, single layer and unidirectional radiation pattern and shows all favorable conditions for off-body communication in body area network.

REFERENCES

1. Liu, Z. G. and Y. X. Guo, "Dual-band low profile antenna for body Centric communications," *IEEE Trans. Antennas. Propag.*, Vol. 61, No. 4, 2282–2285, 2013.
2. Chi, Y. J. and F. C. Chen, "On-body Adhesive-bandage-like antenna for wireless medical telemetry service," *IEEE Trans. Antennas Propag.*, Vol. 62, 2472–2480, 2014.
3. Kang, D. G., J. Tak, and J. Choi, " Lowprofile dipole antenna with parasitic elements for WBAN applications," *Microw. Opt. Technol. Lett.*, Vol. 58, No. 5, 1093–1097, 2016.
4. Raad, H. K., H. M. Al-Rizzo, A. I. Abbosh, and A. I. Hammoodi, "A compact dual band polyimide based antenna for wearable and flexible telemedicine devices," *Progress In Electromagnetics Research C*, Vol. 63, 153–161, 2016.
5. Chen, Y. S. and T. Y. Ku, "A low-profile wearable antenna using a miniature high impedance surface for smartwatch applications," *IEEE Antennas Wirel. Propag. Lett.*, Vol. 15, 1144–1147, 2015.
6. Lacik, J., T. Mikulasek, Z. Raida, and T. Urbanec, "Substrate-Integrated waveguide monopolar ring-slot antenna," *Microw. Opt. Technol. Lett.*, Vol. 56, 1865–1869, 2014.
7. Luo, G. Q., Z. F. Hu, L. X. Dong, and L. L. Sun, "Planar slot antenna backed by substrate integrated waveguide cavity," *IEEE Antennas Wirel. Propag. Lett.*, Vol. 7, 236–239, 2008.
8. Liu, W. C. and C. S. Chen, "Design of missile-mounted SIW antenna with high directivity for data transmission," *Progress In Electromagnetics Research C*, Vol. 38, 79–88, 2013.
9. Khan, A. A. and M. K. Mandal, "Miniaturized substrate integrated waveguide (SIW) power dividers," *IEEE Microw. Wirel. Compon. Lett.*, Vol. 26, No. 1, 888–890, 2016.

10. Khan, A. A., Mandal, M. K., "Dual-band substrate integrated waveguide filter with independently controllable bandwidth," *Asia-Pacific Microwave Conference (APMC)*, 1–4, 2016.
11. Liu, X., H. Song, C. Zhong, Y. Chen, and T. Luo, "Design of differential-mode bandpass filters on SIW structure," *Progress In Electromagnetics Research*, Vol. 72, 69–74, 2018.
12. Kumar, A. and S. Raghavan, "Wideband slotted substrate integrated waveguide cavity-backed antenna for Ku-band application," *Microw. Opt. Techol. Lett.*, Vol. 59, 1613–1619, 2017.
13. Razavi, S. A. and M. H. Neshati, "Development of a linearly polarized cavity-backed antenna using HMSIW technique," *IEEE Antennas Wirel. Propag. Lett.*, Vol. 11, 1307–1310, 2012.
14. Chaturvedi, D. and S. Raghavan, "A dual-band half-mode substrate integrated waveguide-based antenna for WLAN/WBAN applications," *International Journal of RF and Microwave Computer-Aided Engineering*, DOI: 10.1002/mmce.21239, 2018.
15. Agneessens, S. and H. Rogier, "Compact half diamond dual-band textile HMSIW on body antenna," *IEEE Trans. Antennas Propag.*, Vol. 62, No. 5, 2374–2381, 2014.
16. Jin, C., R. Li, A. Alphones, and X. Bao, "Quarter-mode substrate integrated waveguide and its application to antennas design," *IEEE Trans. Ant. Propag.*, Vol. 61, No. 6, 2921–2928, 2013.
17. Chaturvedi, D. and S. Raghavan, "Circular quarter-mode SIW antenna for WBAN application," *IETE J Res.*, 1–7, 2017, Doi: 10.1080/03772063.2017.1358115.
18. Sam, S. and S. Lim, "Electrically small eighth-mode substrate-integrated waveguide (EMSIW) antenna with different resonant frequencies depending on rotation of complementary split ring resonator," *IEEE Trans. Antennas Propag.*, Vol. 6, No 10, 4933–39, 2013.
19. Hong, G. Y., J. Tak, and J. Choi, " An all-textile SIW cavity-backed circular ring-slot antenna for WBAN applications," *IEEE Antennas Wirel. Propag. Lett.*, Vol. 15, 1995–1999, 2016.
20. Moro, R., S. Agneessens, H. Rogier, and M. Bozzi, "Wearable textile antenna in substrate integrated waveguide technology," *Electronics Letters*, Vol. 48, No. 16, 985–87, 2012.
21. Lajevardi, M. E. and M. Kamyab, "A low-cost wideband quasi-yagi SIW-based textile antenna," *Progress In Electromagnetics Research*, Vol. 67, 53–59, 2017.